Non-inductive Plasma Current Start-up by EC and RF Power in the TST-2 Spherical Tokamak

A. Ejiri, Y. Takase, J. Sugiyama, T. Oosako, T. Yamaguchi, Y. Adachi, O. Watanabe, T. Masuda, M. Sasaki, H. Tojo, S. Kainaga, Y. Nagashima, B. I. An, H. Kobayashi, H. Kurashina, H. Hayashi, H. Matsuzawa and K. Yamada

The University of Tokyo, Kashiwa 277-8561, Japan

e-mail contact of main author: ejiri@k.u-tokyo.ac.jp

Abstract. Non-inductive plasma current start-up by EC and RF power was carried out on the TST-2 device. Low frequency RF (21 MHz) sustainment was demonstrated, and the obtained high β_p spherical tokamak configuration has similar equilibrium values as the EC (2.45 GHz) sustained plasma. Equilibrium analysis revealed the detailed information on three discharge phases: (i) In the initial current formation phase, linearity between the plasma current and the stored energy was confirmed. (ii) In the current jump phase, the initial closed flux surfaces cause a change in the current increasing rate, but the stored energy does not show such a change. (iii) The current sustained plasma is characterised by the fraction of the current inside the last closed flux surface to the total current, and the fraction seems to determine the ratio of the plasma current to the external vertical field. MHD instabilities often terminate the RF sustained plasma, but no such phenomenon was observed in the EC sustained plasma.

1. Introduction

Key issues in spherical tokamak (ST) research are plasma current I_p start-up and formation of the ST configuration without the use of a central solenoid (ohmic coil). Successful current generation, ST formation and sustainment have been achieved by injecting RF power (usually in the EC frequency range) to a configuration with a toroidal field and a weak vertical field. This scenario was developed in CDX-U using EC waves [1], and similar experiments were performed in the ST devices: LATE [2,3], TST-2@K [4], TST-2 [5], CPD [6], MAST [7]. A clear transition from open field line configuration to ST configuration, accompanied by a rapid increase in I_p (so called current jump), was found in LATE. This phenomenon was also observed in TST-2 and in CPD. Experiments in these devices suggest that a higher vertical field B_z and a higher EC power are preferable to achieve a higher I_p as long as a current jump occurs. However, the current formation mechanism and the ST formation mechanism are still not clearly understood. Especially, equilibrium reconstruction was performed for only one case [4], and the time evolution and the variation in different operations remain unknown. The mechanisms for ST formation and the features of the plasma should be identified to extrapolate present results to next step ST devices. In TST-2, effects of various operational parameters are studied in [8]. It was found that the sustained current is roughly proportional to the vertical field strength B_z, but dependences on other parameters are very weak. On the other hand, the initial current ramp-up rate depends on several parameters, and a scaling law was obtained. A current jump occurs when the initial current reaches a value proportional to B_z, and the value is consistent with the condition to form closed flux surfaces. Recently, a low frequency RF source (21MHz) was used, and ST configuration was sustained by a non-EC heating method for the first time [9]. There is a threshold in the RF power, and the threshold for deuterium plasma was lower than that for hydrogen plasmas. In this paper, the three discharge phases (formation, jump, and sustainment of the plasma current) were analyzed, and equilibrium reconstruction was performed in each phase. It was found that the start-up plasma is characterized by high β_p, and a spontaneous transition from an open field line configuration to a partially closed field line configuration. Various aspects of the equilibrium

and the dynamics are revealed, and the potential of the start-up plasma as a transient state to a reactor relevant plasma is described.

2. TST-2 Device and the Wave Heating Systems

TST-2 is a spherical tokamak with the following typical parameters [10]: major radius $R < 0.38$ m, minor radius $a < 0.25$ m, aspect ratio $A = R/a > 1.5$, toroidal magnetic field $B_t < 0.3$ T, and plasma current $I_p < 140$ kA (inductive operation). Five poloidal field coil sets (PF1, PF2, PF3, PF4, PF5) are installed to produce various vertical field configurations. In this study, a moderate mirror configuration (with a vertical field index $-d\ln B_Z/d\ln R=0.73$ at R=0.38 m) was generated using the PF1 and PF2 coils. EC power (2.45 GHz, up to 5 kW) was injected from the low field side along the major radius in X-mode polarization. The fundamental EC resonance layer exists in the vacuum vessel. RF power (21 MHz, up to 30 kW) was injected using a loop antenna, which is normally used for exciting the high harmonic fast wave (HHFW) in ohmic plasmas. The antenna has two current straps, but only one strap was used in this study. According to the calculated wave dispersion, in the low density ($\sim 1\times10^{17}$ m^{-3}) start-up plasmas, majority of the power of the excited fast wave with toroidal mode numbers of order 10 is evanescent, and only a small fraction of the power with low toroidal mode numbers can propagate into the core. This is consistent with the observation of poor antenna loading. The difference between the antenna loadings with/without plasma indicates that about one third of the power delivered to the antenna is radiated into the antenna. Deuterium was used in this study, because of its lower RF power threshold for the current sustainment [9]. Since the RF frequency is much higher than the deuterium cyclotron frequency, ion heating is not expected, and no deuterium or impurity heating was observed in the Doppler profiles. On the other hand, high energy electrons can be heated by the HHFW, and the high energy tail around 2 keV was observed in the soft X-ray spectra when the injected RF power is as high as 30 kW. It should be noted that a (directional) current drive is not expected for either wave because of poor single pass absorption. As described above, we can expect electron heating by both waves (EC and HHFW), and the symptoms of heating were observed. The equilibrium reconstruction enabled the estimation of the temperature.

3. Experimental Results and Equilibrium Reconstruction

Figure 1 shows waveforms of a typical EC start-up discharges. Two discharges are over plotted. EC alone was used in one discharge (black curves), and in the other (red curves), the heating wave was switched from EC to RF with a short overlapping period (30-42 ms). Three phases can be identified: (i) the initial current formation phase, in which I_p increases gradually, (ii) the current jump phase around the vertical lines shown in Fig.1, and (iii) the current sustainment phase. These phases are described separately in the following subsections. The equilibrium configurations were reconstructed through a least square fit of a parameterized equilibrium to the magnetic measurements of about 80 channels. A truncated equilibrium, which was first introduced to analyze the equilibrium of the TST-2@K plasma [4], was used. In the truncated equilibrium, finite current density and pressure gradient exist outside the last closed flux surface (LCFS). The LCFS is determined in practice by the inboard limiter in these experiments and the region outside the LCFS is a SOL region bounded by the outboard limiter. The field lines in this region hit the other limiters (i.e., top, bottom or inboard limiters). Thus, the current density and the pressure in this region are truncated at these limiters. The truncated equilibrium was necessary to reconstruct the TST-2@K equilibrium, which is characterized by a very high ratio of I_p/B_z=4 kA/2 mT. Since the equilibrium includes the open field line region, it is also useful to express the dynamics of the

equilibrium during the first two phases (i), (ii). In this study the following expression is used for the toroidal current density j_ϕ, which is different from that used in [4],

$$j_\varphi = R\frac{dp}{d\psi} + \frac{\mu_0}{R} f \frac{df}{d\psi} = j_0(1-\psi)\left(\beta_{p0}\frac{R}{r_0} + (1-\beta_{p0})\frac{r_0}{R}\right),$$

where β_{p0} is the most significant fitting parameter. j_0 and r_0 are the normalization values. The plasma current, the poloidal field current and the eddy current through the vacuum vessel are the other (minor) fitting parameters. Other expressions such as $1-\psi^2$ can be used, and the fitting was not so poor in phase (iii), but the above expression $1-\psi$ was adopted, because it yields relatively good fitting throughout a discharge. The eddy current in the vacuum vessel wall due to the varying plasma current was included in the calculation, to improve the fitting during the current jump phase.

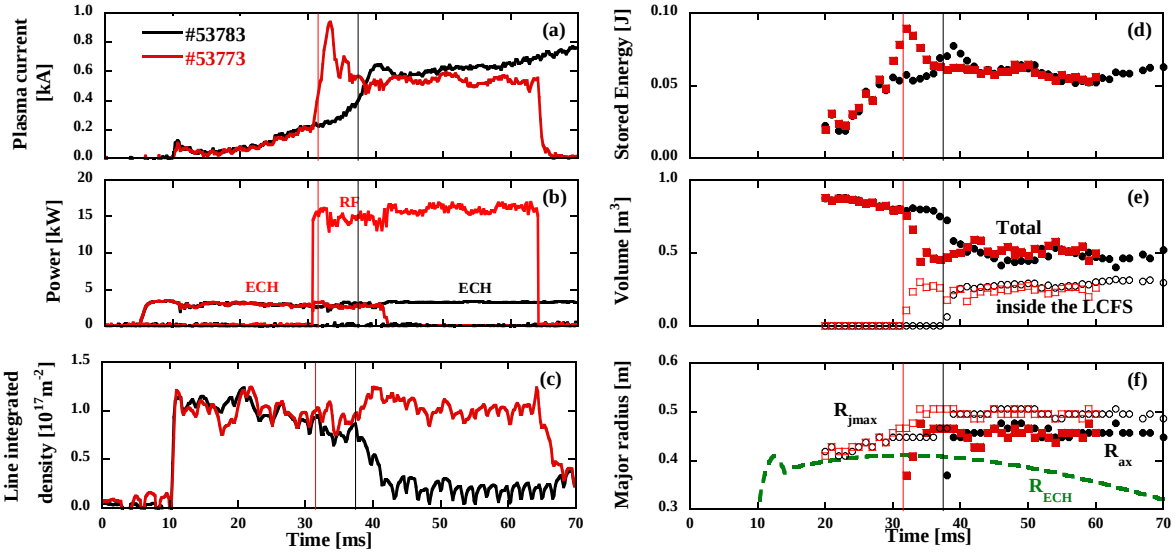

FIG. 1. Discharge waveforms for an EC sustained discharge (black) and an RF sustained discharge (red); plasma current (a), injected power (b), line integrated density at R=0.39 m (c), stored kinetic energy (d), total volume and the volume inside the LCFS (e), and major radii of the current density peak R_{jmax}, magnetic axis R_{ax} and the radius of the fundamental ECH resonance layer R_{ECH} (green) (f) are shown.

3.1. Initial Current Formation Phase

The current in the initial current formation phase is very small, and no closed flux surface is formed (Fig. 2(d)). In this phase, unidirectional toroidal precession of mirror trapped electrons is believed to contribute to the current. According to the theory described in [11], the current due to the trapped electrons is proportional to the stored energy. The relationship was confirmed by the evolution of the stored energy as long as the current is small (20-30 ms in Fig. 1 (d), Fig. 3). It should be noted that the pressure driven current also yields a similar relationship and we cannot distinguish the current generation mechanisms by the waveform of the stored energy alone [11]. The volume of the plasma (i.e., volume inside the truncated boundary) decreases gradually, while the radius for the current density peak increases gradually (Fig.1(f)). Since the boundary is determined mainly by the outboard and the inboard limiters, the decrease in the volume was accompanied by the decrease in the height. Note that the current density peak was located close to the radius for the EC fundamental resonance layer. For EC injection alone, a current jump occurs when the current reaches a value

determined by the external B_z [8]. Therefore, the current ramp-up rate is an important parameter to induce a current jump within a finite discharge duration. The dependences of the ramp-up rate on various parameters were investigated and a scaling law was obtained [8]. In contrast to the ECW injection alone, RF injection causes a current jump even if the current is lower than the value as long as the injected power exceeds a threshold [9].

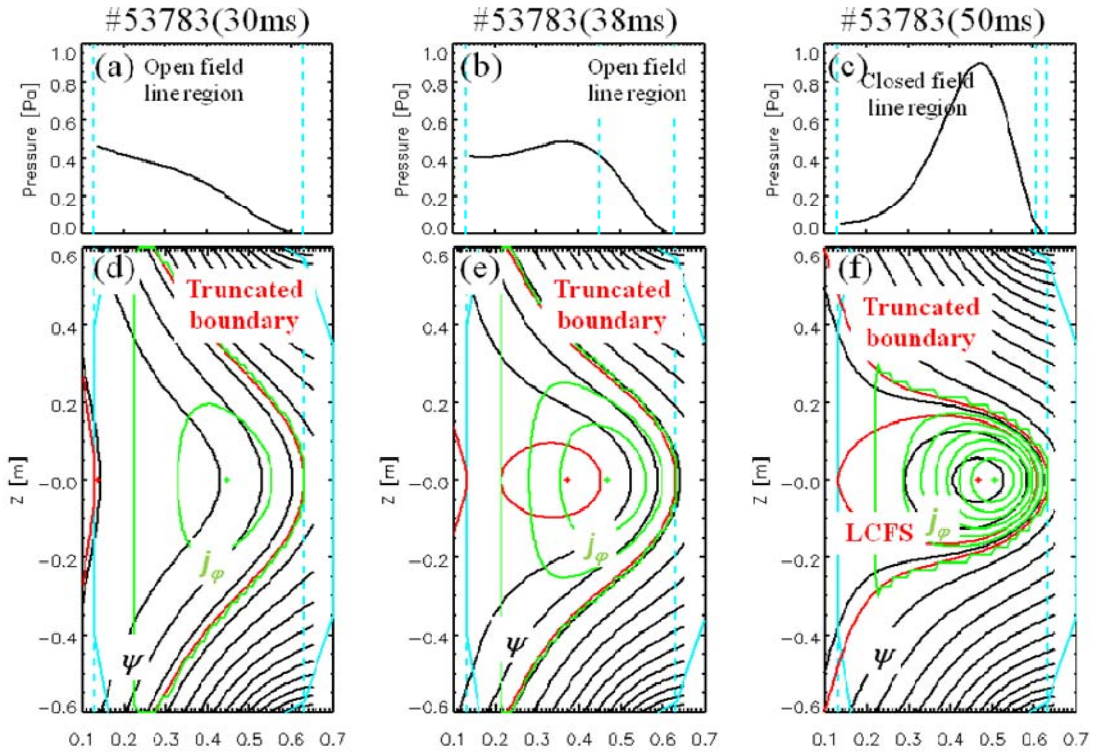

FIG. 2. Reconstructed pressure profiles (a), (b), (c) and flux surfaces (d), (e), (f) during the three discharge phases. Contours for the toroidal current density (green) are also plotted. The red contours indicate the flux surface which just touches the inboard or the outboard limiter at Z=0, and the surface corresponds to either the LCFS or the truncated boundary, except for the case of LCFS in Fig. (e).

3.2. Current Jump Phase

The current jump is a phenomenon found in LATE [2], and observed in other experiments. It is a spontaneous transition from an open field line configuration to an ST configuration with closed flux surfaces. It is believed that the confinement of the current carrying particles is improved as soon as closed flux surfaces are formed, and the improved confinement induces a rapid current increase. However the details such as timing and temporal evolution of the configuration were unknown.

The vertical lines in Fig.1 indicate the timings of the initial closed flux surface formation. In the case of ECH alone (black curves in Figs. 1, 3), the slope of the plasma current changed at this timing. In addition, the plasma volume showed a rapid decrease. The radius of the current density peak R_{jmax} showed little change, and the stored energy continued increasing and then started to decrease (see Fig. 1(d) 40 ms in the black curves), and the plasma current also started to decrease. Similar behavior can be seen for the RF injected discharge (red curves in Fig. 1), but the current ramp-up rate was too fast to identify a change in the slope. These experimental results agree partly with what we have believed. The rapid changes in the

current and the shape imply an important role of the closed flux surfaces. However, the little change in the stored energy implies that the improvement in the confinement is not required for a jump. The differences between the current/shape evolutions and the stored energy evolution necessitate a more accurate and detailed understanding of the current jump mechanism. Using the equilibrium values we can estimate the global energy confinement time and the current penetration time. These are of orders 10 μs and 1 ms, respectively, and the time scale for the current jump agrees with the latter (i.e., current penetration time). The current ramp-up rate during a jump induced by RF power increases with the injected RF power [9], and the dependence is qualitatively reasonable. However a much shorter global energy confinement time implies the efficiency in converting the RF power to the plasma current is poor. The little change in the position of the peak current density (see Fig.1(f) and Fig.2(d),(e)) implies a quiet transition rather than a violent transition (i.e., dynamics) seen in the merging or the CHI experiments. Thus, we cannot expect and could not observe ion heating due to magnetic reconnection.

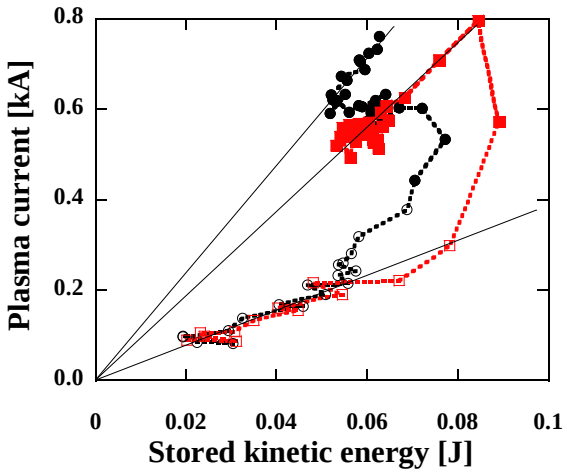

FIG. 3. Discharge trajectories in the plane of the stored energy and the plasma current for an EC sustained discharge (black) and an RF sustained discharge (red). Open symbols represent the data when closed flux surfaces are not formed, and closed symbols represent the data when closed flux surfaces exist. Three thin black lines are guides to show the linear relationship between the stored energy and the plasma current.

3.3. Current Sustainment Phase

After a current jump, closed flux surfaces exist and the plasma current I_p is sustained. The value of I_p is roughly proportional to B_z, but dependences on other parameters such as the injected EC power, EC wave polarization, and vertical field configuration are very weak [8]. In these experiments, contribution of EBWCD cannot be excluded because EBW is strongly absorbed. Figure 1 demonstrates that a similar I_p can be sustained by RF power at 21 MHz. As in the case of EC sustainment, I_p does not depend on the RF power as long as the power is larger than the threshold power.

An equilibrium during the EC sustained phase is shown in Fig. 2 (c), (f). The major radii for the magnetic axis and the current density peak are R_{ax}=0.47 m, R_{jmax} =0.51 m. The central pressure (p_0~0.9 J) corresponds to the electron temperature of about T_{e0}~100 eV, here we used the line averaged density and the central pressure. The plasma cross section is characterized by a low elongation factor κ~0.7. The central safety factor is q_0~30. Poloidal beta β_p is a measure of the normalized pressure, and it is an important value when we study

MHD stability. Here β_p is defined by the volume averaged pressure divided by magnetic energy $\overline{B}_p^2/2\mu_0$, where $\overline{B}_p = \mu_0 I_p / l_{boundary}$, and we take the volume inside the LCFS for the averaging and for the poloidal perimeter $l_{boundary}$. β_p for Fig. 2 (c), (f) was about 1.0. The fraction of the plasma current inside the LCFS to the total current was I_{LCFS}/I_p~99%. The values for the RF sustained discharge at the same timing (t=50 ms) were R_{ax}=0.47 m, R_{jmax} =0.51 m, p_0~0.8 J, T_{e0}~25 eV, q_0~40. β_p~1.2 and I_{LCFS}/I_p~92%. The temperature was much lower than that for the EC sustained plasma, because of the higher density. The parameters to characterize the shape of the plasma are almost identical to those of the EC sustained plasma. As shown in Fig. 3, not only during phase (i), but also in the sustainment phase (iii), the trajectory tends to follow a linear relationship between I_p and the stored energy W, but the coefficients were different. The EC sustained plasma lasted until t=90 ms, and I_p and W increased gradually, while R_{ax}, R_{jmax} and I_{LCFS}/I_p remained almost constant. These results suggest that the sustained plasma has its own state characterized by I_p/W or I_{LCFS}/I_p.

When we analyze various discharges, the sustained current is almost proportional to the external vertical field strength, and the ratio I_p/B_z is a quantitative value to characterize the sustained plasma. The ratio for the sustained plasmas (shown in Figs. 1, 2) was I_p/B_z =1.1 kA/mT, and the ratio is similar to those obtained in CDX-U, LATE and CPD, which are similar in plasma size. However, the value in TST-2@K was I_p/B_z =2 kA/mT [4] which is about twice higher than the present value. Figure 4 shows another EC sustained discharge with stronger B_z. The equilibrium values were I_p=1.3 kA, p_0~1.4 Pa, T_{e0}~180 eV, q_0~50. β_p~1.1, I_{LCFS}/I_p~66% and I_p/B_z =1.5 kA/mT. Thus, this I_p/B_z is located in the middle of that for the above discharges and that for the TST-2@K discharge. The differences of I_p/B_z between these discharges can be interpreted from the view point of equilibrium. The equilibrium in TST-2@K was characterized by a low current fraction inside LCFS, I_{LCFS}/I_p~25% (I_p/B_z =2 kA/mT), while the fractions for discharges shown in this paper are I_{LCFS}/I_p~66% (I_p/B_z =1.5 kA/mT) and I_{LCFS}/I_p>90% (I_p/B_z =1.1 kA/mT). These results suggest that the current fraction should be low to achieve an equilibrium with a high I_p/B_z, and that a large variation in I_p can be obtained for a given B_z for the truncated equilibrium. The large I_p/B_z on TST-2@K is probably attributed to the very high EC power.

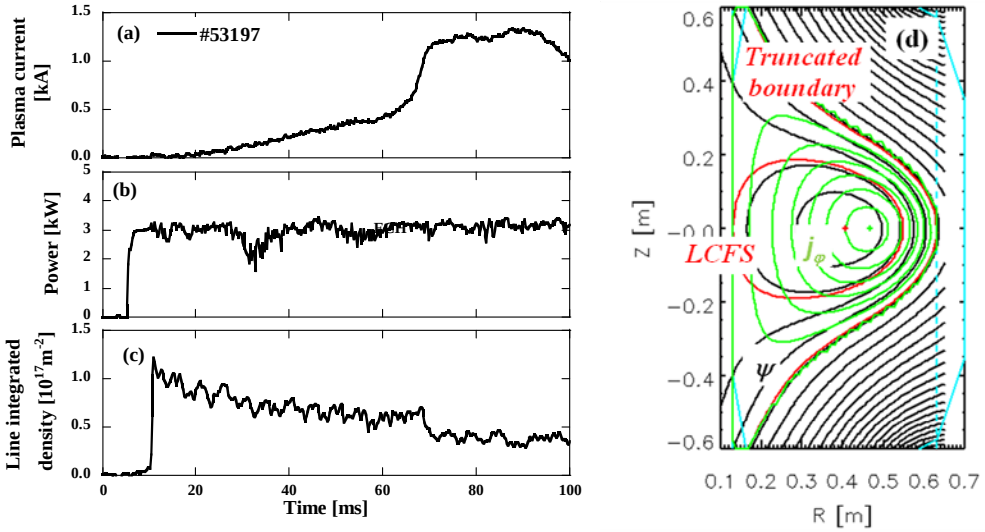

FIG. 4. EC sustained discharge waveforms; plasma current (a), ECH injected power (b) and the line integrated density (c) are shown. Figure (d) shows the reconstructed configuration at t=90 ms.

The EC sustainment lasts until the fundamental resonance layer disappears from the vacuum vessel. The minimum toroidal field strength for the RF sustainment was less than half of that for the EC sustainment [12]. This fact implies that RF could be a more flexible tool for start-up experiments than ECW. However, the RF sustained plasma current often disrupts and the current relaxes to a low value (e.g. 0.2 kA), and closed flux surfaces are lost. Note that the relaxed current value is almost the same as the value obtained by RF alone (without the initial ECH). Due to the large β_p, it is possible that MHD instabilities disrupt the plasma. Figure 5 shows four discharges with current disruption and one discharge without disruption (solid black curves). Operational conditions were almost the same. An EC sustained discharge (dotted black curve) is also plotted. Power of the high frequency magnetic fluctuations (> 5 kHz) measured by pick-up coils located near the inboard midplane and near the outboard midplane are shown. The fluctuations are normalized by the DC external vertical field strength. The inboard fluctuations increased rapidly from about 1 ms before the start of the current drop (Fig. 5(b)). The outboard fluctuations seem to show a similar but more obscure behavior, due to higher background (i.e., constant) fluctuation level (Fig. 5(c)). The power spectra are enhanced for the disrupted discharge in the frequency ranges 5-10 kHz, and below about 1 kHz (Fig. 5(d)). The low frequency components (< 1 kHz) exist from the beginning of the sustainment phase (t > 35 ms) for the disrupted discharges. In addition, the calculated R_{ax} starts to move inward about 2 ms before the current disruption. These results suggest that the current disruption is induced by the fast MHD activities, and that the low frequency fluctuations and the inward shift of the magnetic axis destabilize the equilibrium configuration. It should be noted that the EC sustained discharge has much lower fluctuation levels.

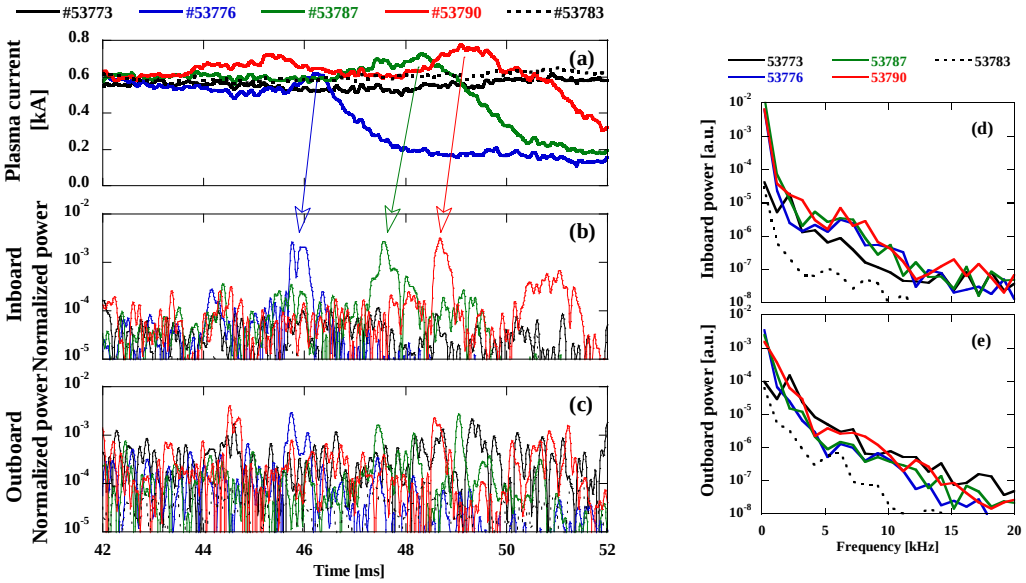

FIG. 5. Time evolutions of five discharges; plasma current (a), powers of the inboard magnetic fluctuations (b) and outboard magnetic fluctuations (c) are shown. Figs. (d), (e) show the power spectra for the same time window shown in (b) and (c).

4. Conclusions

Non-inductive plasma current start-up by EC and RF power was carried out on the TST-2 device. Plasma current sustainment by low frequency RF power was demonstrated, and the obtained high β_p ST plasma was found to have similar equilibrium properties as the EC sustained plasma. Equilibrium analysis revealed detailed information during each phase of discharge. The initial current formation phase is characterized by a slow increase in the current, proportional to the stored energy. In the current jump phase, the current ramp-up rate (i.e., slope) changes when the initial closed flux surfaces are created in the plasma, while the stored energy does not show such a change in slope. The configuration of the sustained plasma seems to be characterized by the current fraction inside the LCFS (I_{LCFS}/I_p), and the fraction seems to determine the operational ratio I_p/B_z. MHD instabilities often terminate the RF sustained plasma, but no such phenomena were observed for the EC sustained plasma. Although MHD stability is an important issue, the variety of the sustained plasmas, and non-EC sustainment tool were demonstrated. These might initiate clarification of rich physics in the start-up plasmas and might lead to flexible start-up scenarios to a reactor relevant plasma.

Acknowledgments

This work is supported by Japan Society for the Promotion of Science under Grant-in-Aid for Scientific Research No. 16106013, and by National Institutes for Fusion Science NIFS07KOAR008 and NIFS07KUTR02.

References

[1] Forest, C. B., et al., Phys. Rev. Lett. **68**, 3559 (1992).
[2] Yoshinaga, T., et al., J. Plasma Fusion Res. **81**, 333 (2005).
[3] Maekawa, T., et al., Nucl. Fusion. **45**, 1439 (2005).
[4] Ejiri, A., et al., Nucl. Fusion **46**, 709 (2006).
[5] Ejiri, A., et al., Trans. Fusion Sci. Tech. **51, No.2T**, 168 (2007).
[6] Kikukawa, T., et al., Plasma Fusion Res. **3**, 010 (2008).
[7] Lloyd, B., et al., 13th International Workshop on Spherical Torus 2007 10 - 12 Oct 2007, Fukuoka, Japan. http://www.triam.kyushu-u.ac.jp/ISTW2007/agenda.html ,
[8] Sugiyama, J., et al., Plasma Fusion Res. **3**, 026 (2008).
[9] Watanabe, O., et al., Plasma Fusion Res. **3**, 049 (2008).
[10] Takase, Y., et al., Nucl. Fusion **41**, 1543 (2001).
[11] A.Ejiri and Y. Takase., Nucl. Fusion **47**, 403 (2007).
[12] Watanabe, O., et al., submitted to Plasma Fusion Res.